This is a Just Accepted version, keep updated with https://doi.org/10.26599/CS.2026.9510010

CS 2026, 2, 9510010

Research Article

https://doi.org/10.26599/CS.2026.9510010

# Fine-resolution carbon dynamics mapping reveals unequal contributions to carbon neutrality within Chinese cities

Lixing Wang[1], Zongyao Sha[2], Tao Li[1], Taochun Sun[1]

1 Department of Earth System Science, Tsinghua University, Beijing 100084, China

2 School of Remote Sensing and Information Engineering, Wuhan University, Wuhan 430072, China

Address correspondence to Lixing Wang, wanglx23@mails.tsinghua.edu.cn

Received: May 5, 2025 / Revised: May 15, 2025 / Accepted: June 3, 2026

Abstract

Understanding the inequalities of carbon neutrality within cities is essential for implementing differentiated carbon reduction policies. Here we develop an integrated model to conduct a fine-resolution (250-m, monthly) assessment of net carbon emissions (NCE) for three major urban agglomerations in China. Our results precisely depict the seasonal patterns of NCE and highlight the diverse urban carbon dynamics that contribute to inequalities in carbon neutrality. Nearly half of the 48 cities exhibited NCE exceeding 1000 $gC \cdot m^{-2} \cdot a^{-1}$, while only 5 cities functioned as carbon sinks. Theil index (T) analysis reveals that intra-city inequalities are more pronounced in industrial cities (T＞0.11), while inter-city disparities are primarily driven by economic and industrial imbalances, particularly in the Pearl River Delta, where T has reached 0.18. This emphasizes the dominant role of high-emission cities in shaping regional inequalities. These findings provide actionable insights for urban afforestation and emission mitigation policies aimed at achieving carbon neutrality.

Keywords: Superior resolution; carbon neutrality inequality; net carbon emissions; carbon sink; CASA model; Theil index

Main body

1 Introduction

Clarifying the level of carbon neutrality and its inequality within cities is crucial for implementing targeted carbon reduction policies and coordinating regional development. Urban areas account for over 80% of anthropogenic carbon emissions in China, and by 2020, the country's urbanization rate had exceeded 60% [1, 2]. This rapid urban expansion has had complex impacts on regional carbon sources and sinks, exacerbating the inequalities in achieving carbon neutrality within cities and posing significant challenges to monitoring urban carbon dynamics. The difference between carbon emissions and sinks, defined as net carbon emissions (NCE) [3, 4], serves as a key indicator for evaluating the effectiveness of urban strategies aimed at achieving carbon neutrality. Dynamic monitoring of NCE at finer spatiotemporal scales facilitates a quantitative assessment of carbon source-sink disparities [5]. It deepens our understanding of the spatiotemporal heterogeneity in urban carbon budgets, which is fundamental to deciphering the unequal contributions of various urban areas to carbon neutrality. The insights derived are therefore critical for guiding targeted interventions in urban afforestation and industrial emission regulation, enabling a strategic pathway toward effective carbon neutrality management.

Existing studies estimate that China's terrestrial ecosystem carbon sinks have offset approximately 7-15% of anthropogenic CO_2 emissions since 2010 [6], with nearly half of China's provinces offsetting less than 10% of CO_2 emissions through terrestrial carbon sinks [7]. However, current methodologies for quantifying carbon sinks and emissions often lack precision and accuracy. Systematic assessments of China's progress toward urban carbon neutrality at finer spatiotemporal scales are still lacking. Consequently, most studies on carbon neutrality inequalities have focused on scales above the city level, limiting their ability to delve deeper into intra-urban discrepancies. For instance, previous research has employed models such as the Gini coefficient, Kakwani index, and Theil index, specifically designed to quantify inequalities [8-10], to assess the uneven distribution of provincial carbon emission intensities or NCE, revealing patterns of disparity within and between provinces. Due to the significant spatial heterogeneity in industrial structures and urban greening within cities, carbon reduction policies require tailored decision-making, underscoring the urgent need for high-resolution NCE accounting to guide effective policy implementation.

To effectively evaluate NCE, it is essential to accurately and finely determine ecosystem carbon sinks and anthropogenic carbon emissions. When not taking natural disturbances into account, net ecosystem productivity (NEP) can be considered as ecosystem carbon sink [11], which is calculated by subtracting soil heterotrophic respiration from vegetation's net primary productivity (NPP). Remote sensing, combining data with ecological models, is a widely used method for estimating terrestrial carbon sinks. It offers broad coverage and long-term data compared to traditional methods like inventory and eddy covariance [12]. Various models use remote sensing and meteorological data for carbon sink estimation [13-16]. Models vary in applicability and are influenced by the specific vegetation characteristics of different areas.

Currently, the commonly used models include CASA model, 3-PG model, InVEST model, etc. Among them, the CASA (Carnegie-Ames-Stanford Approach) model has been widely used by scholars due to its advantages of fewer parameters involved, broad applicability, and high accuracy. Previous studies using the CASA model to estimate China's annual NPP changes showed strong consistency between simulated and observed values, with coefficient of determination (R^2) over 0.7 [17, 18]. Generally, current NPP research tends to provide annual results with coarse resolution (>1km), which cannot sensitively capture the intricate variations in carbon sinks within urban environments.

Regarding the accounting of carbon emissions, due to the scarcity of statistical data, current research on establishing emission inventories is limited mainly to annual data at the national and provincial levels with delayed update frequencies [19-21]. Presently, emission inventories at the city level or more granular scales are still incomplete. By using specific spatial proxy data, it is possible to disaggregate coarse scale carbon emission inventories into fine grid level data. For example, since nighttime light (NTL) intensity partially reflects the level of local economic activity and industrialization, it is reasonable to employ NTL data to model carbon emissions stemming from human activity [22-25]. However, NTL data has limitations; it only identifies emissions in lit areas, missing emissions from unlit areas where over 1.6 billion people live [26]. Additionally, it mainly captures point source emissions and does not account for nonpoint sources like traffic. The level of urbanization and complexity of economic activities in different areas also lead to deviations between the actual values of CO_2 emissions and fitting results from NTL data. Liu et al. [27] divided the study area into lit and unlit areas, and used NTL data and population grid density as distribution factors for more accurate regional emission mapping, but the disaggregation algorithm is not reasonable enough and the distribution of nonpoint source emissions has not been considered. A more comprehensive and scientific disaggregation model needs to be proposed.

In this case study, we developed an integrated model to quantify NCE at 250m scale and assess its inequalities across three major urban agglomerations (UAs) in China: Beijing-Tianjin-Hebei (BTH), Yangtze River Delta (YRD), and Pearl River Delta (PRD). We combined the CASA model with a soil respiration model to compute the monthly carbon sink changes, thus improving the capture of the dynamic characteristics of urban carbon sinks. Besides, we developed an improved disaggregation method for CO_2 emissions, which makes the spatiotemporal distribution of urban CO_2 emissions more reasonable and accurate. The NCE were derived based on the spatiotemporal distribution of urban carbon sinks and emissions, and we further analyzed the carbon neutrality process and its inequalities using Theil index. In particular, we calculated the unequal contributions of carbon neutrality within cities at the grid level. Finally, the measures and strategies for urban afforestation and emission reduction were discussed.

2 Methods

2.1 Study area

In this study, we selected three major urban agglomerations (UAs) in China as a case study, namely the Beijing-Tianjin-Hebei (BTH) UA, the Yangtze River Delta (YRD) UA, and the Pearl River Delta (PRD) UA. The location map with 30 arc-second population distribution and various types of land cover of the three UAs are shown in Fig. 1. LULC classification data comes from the 10-m classification dataset of China (AIEC) provided by DAMO AI Earth team [28]. All three regions boast diverse vegetation cover, benefitting from ample sunshine and precipitation due to the monsoon climate influence. In addition, these three mega city clusters comprise 33% of the nation's population and contribute a substantial 44% to the country's GDP [29]. They exhibit a notably high level of urbanization, characterized by dense populations and extensive industrial activity in built-up areas. Particularly, we select 10 cities as research focus based on the following criteria: 1. direct-administered municipalities (Beijing, Tianjin, Shanghai), 2. provincial capitals (Shijiazhuang, Hefei, Nanjing, Hangzhou, Guangzhou), and 3. cities with high per capita GDP (Shenzhen, Zhuhai). Investigating the carbon source and sink dynamics in these cities offers valuable insights, given their typicality and representativeness, into the carbon budget features of high-emission urban agglomerations in China.

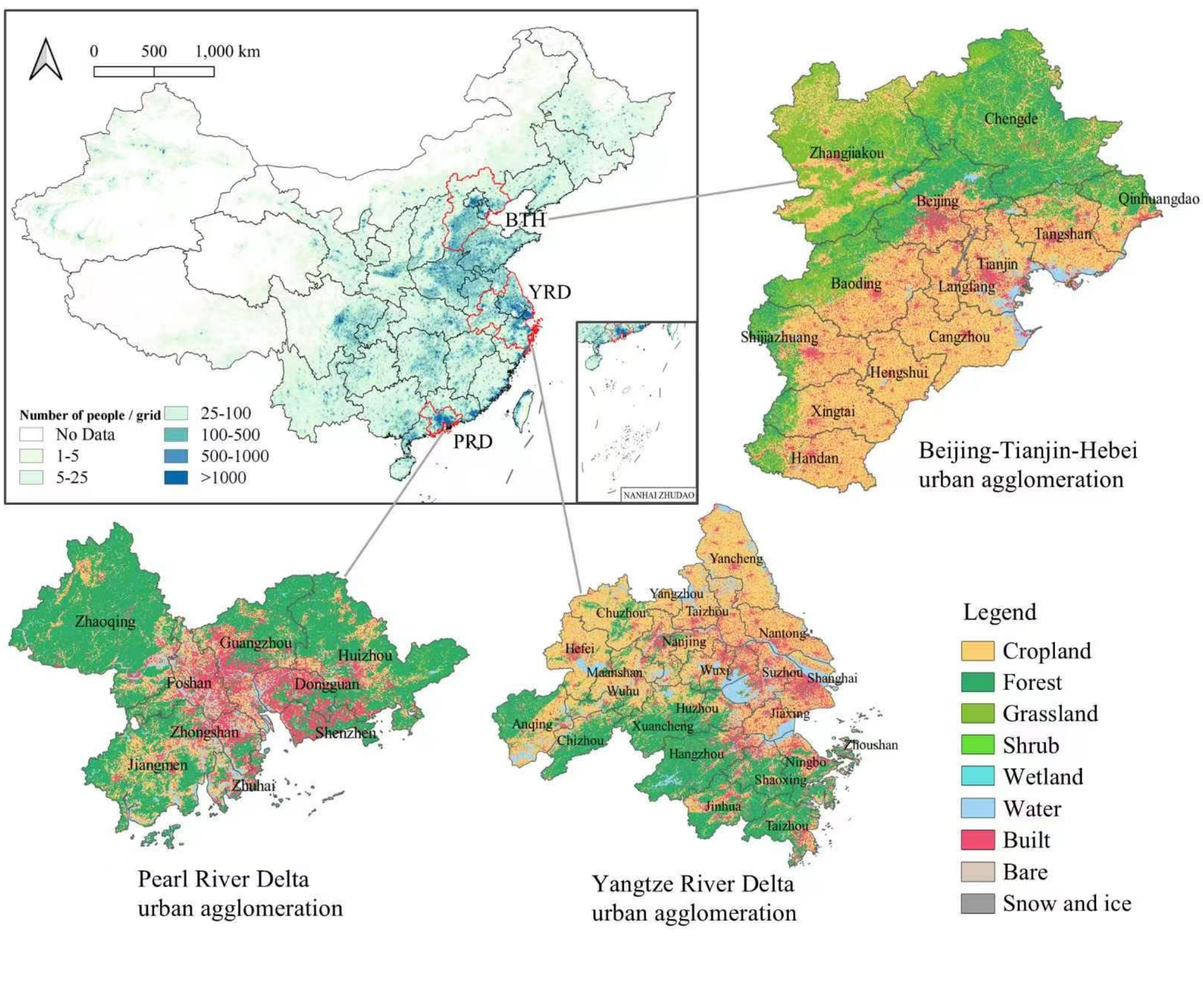

Fig. 1. Location map with population distribution (2020) and land cover classification map of the three major UAs in China (GS 京（2026）2167).

2.2 Data and workflow

We used meteorological and vegetation data to calculate ecosystem carbon sinks, and employed various spatial proxy data to disaggregate provincial carbon emissions (Table 1). The meteorological data we used is ERA5-Land reanalysis dataset [30], which contains the monthly average surface temperature, total solar radiation, soil evapotranspiration and precipitation of global coverage. The Normalized Difference Vegetation Index (NDVI) data is MOD13Q1 v061 product [31] provided by NASA LP DAAC, with a spatial resolution of 250 m, and vegetation type data is reclassified from the GLC_FCS30-2020 land cover dataset [32]. We clipped the images based on the vector boundary of the three UAs and obtained monthly data from 2021 to 2022. We also performed Kriging interpolation on the meteorological data to obtain a spatial resolution that matched the NDVI images for model calculation. The carbon emission data comes from the provincial carbon emission inventory provided by Carbon Monitor team, including point sources (such as power, industry, residential sectors) and nonpoint source sectors (ground transport). LULC, NTL, population and road network density data are used for spatial disaggregation of carbon emissions. The NTL data we used is NPP-VIIRS monthly data [33, 34] from 2021 to 2022, and the population density data is retrieved from the Gridded Population of the World (GPWv4) [35]. The road network density map is converted from the road network shapefile data provided by OpenStreetMap, representing the ratio of the total length of roads within each grid to the grid area.

Table 1. Description and sources of the data used in this study.

Data	Description	Spatial resolution	Source

SOL	Total solar radiation		
T	Temperature of air at 2m above the surface of land	0.1° × 0.1°	ERA5-Land monthly averaged data from Copernicus Climate Data Store (https://cds.climate.copernicus.eu/cdsapp)
E	Soil evapotranspiration		
PR	Precipitation		
NDVI	Normalized Difference Vegetation Index	250m × 250m	MOD13Q1 v061 from NASA Land Processes Distributed Active Archive Center (LP DAAC) (https://lpdaac.usgs.gov/products/mod13q1v061/)
Vegetation type	Vegetation type classification map	30m × 30m	GLC_FCS30-2020 land cover dataset (https://data.casearth.cn/thematic/glc_fcs30/)
PEmis, TEmis	Provincial carbon emissions generated by point and nonpoint sources	/	Carbon Monitor China (https://cn.carbonmonitor.org/)
LULC	LULC classification map	10m × 10m	AI Earth in China (AIEC) (https://engine-aiearth.aliyun.com/#/dataset/DAMO_AIE_CHINA_LC)
NTL	NPP-VIIRS nighttime light data	15″ × 15″	Earth Observation Group, Payne Institute for Public Policy, Colorado School of Mines (https://eogdata.mines.edu/products/vnl/)
Population	population density distribution map	30″ × 30″	Gridded Population of the World (GPWv4) (http://dx.doi.org/10.7927/H49C6VHW)
Road density	Road network density map derived from	500m × 500m	OpenStreetMap of Geofabrik (https://download.geofabrik.de/asia/china.html)

OpenStreetMap

The workflow of our model is shown in Fig. 2. Initially, we use multi-source data to compute the ecosystem carbon sink according to CASA and soil respiration model, then we propose an improved spatial disaggregation model to calculate the distribution of carbon emissions. Finally, we integrate these two parts to derive the spatiotemporal distribution of the net carbon emissions and carry out corresponding carbon neutrality analysis based on Theil index model.

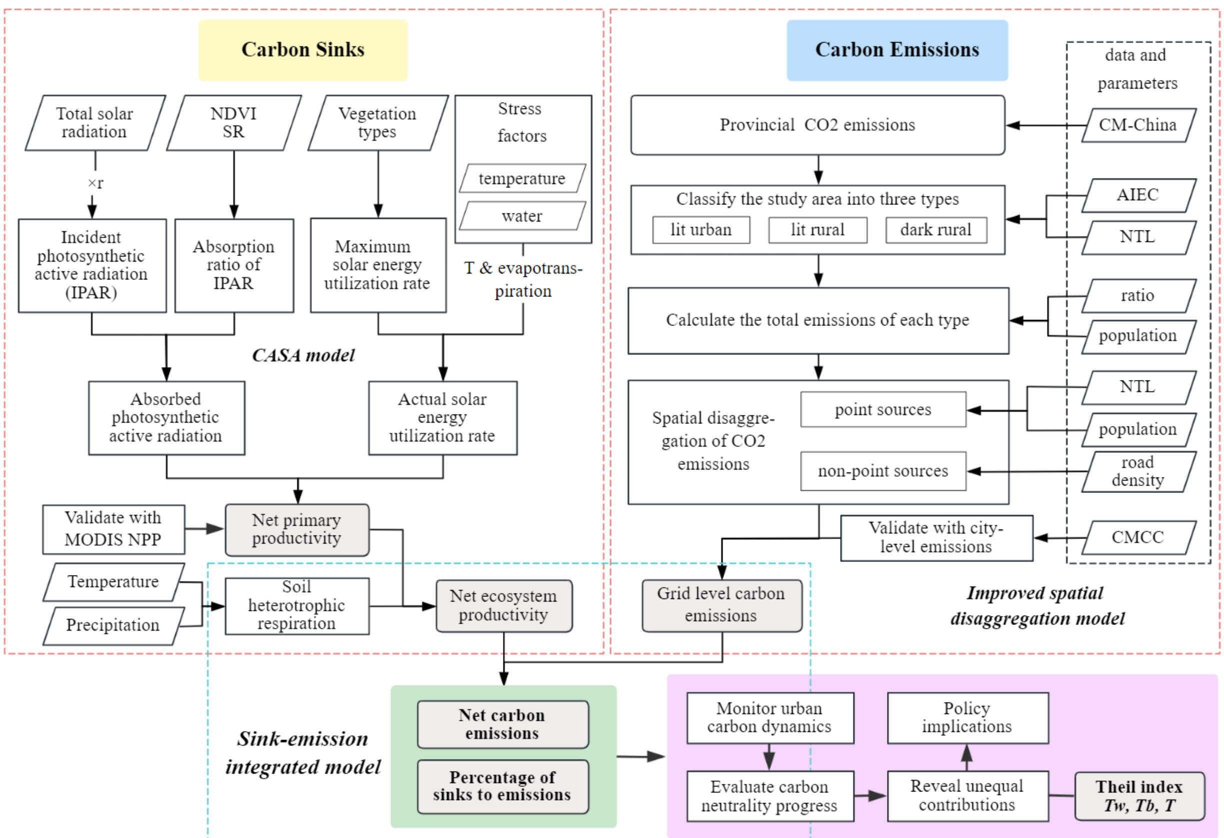

Fig. 2. The workflow of this study.

2.3 CASA model for calculating NPP

The process of calculating NPP using the CASA model is as follows [36, 37]:

$$NPP(x,t) = APAR(x,t) \times \varepsilon(x,t) \quad (1)$$

where $APAR(x,t)$ is the photosynthetic active radiation ($\mathrm{MJ} \cdot m^{-2} \cdot \mathrm{month}^{-1}$) absorbed by pixel x in month t, and $\varepsilon(x,t)$ is the actual solar energy utilization rate ($\mathrm{gC} \cdot \mathrm{MJ}^{-1}$) of pixel x in month t. $APAR$ is calculated as follows:

$$APAR(x,t) = SOL(x,t) \times r \times FPAR(x,t) \quad (2)$$

where $SOL(x,t)$ is the total solar radiation at pixel x in month t, and r is the proportion of incident photosynthetic active radiation (IPAR) utilized by plants (wavelengths 0.4-0.7 μm) to total solar radiation. Research has shown that this parameter can be taken as a constant of 0.5 [38]. $FPAR(x,t)$ is the absorption ratio of vegetation layer to IPAR, which has a linear relationship with the Normalized Difference Vegetation Index (*NDVI*). It is calculated as the following equation, with specific algorithms detailed in Text S1.

$$FPAR(x,t) = \frac{(NDVI(x,t) - NDVI_{i,\min})}{(NDVI_{i,\max} - NDVI_{i,\min})} \times (FPAR_{\max} - FPAR_{\min}) + FPAR_{\min} \quad (3)$$

The actual solar energy utilization rate ε is calculated as follows:

$$\varepsilon(x,t) = T_{\varepsilon 1}(x,t) \times T_{\varepsilon 2}(x,t) \times W_{\varepsilon}(x,t) \times \varepsilon_{\max}(x,t) \quad (4)$$

where $T_{\varepsilon 1}(x,t)$ and $T_{\varepsilon 2}(x,t)$ are low and high temperature stress factors, $W_{\varepsilon}(x,t)$ is water stress factor, reflecting the stress effects of temperature and water conditions on solar energy utilization, respectively. The calculation methods for stress factors are detailed in Text S2. $\varepsilon_{max}(x,t)$ is the maximum solar energy utilization rate ($\mathrm{gC} \cdot \mathrm{MJ}^{-1}$). Potter et al. [15] suggested that the maximum solar energy utilization rate ε_{max} for global vegetation is 0.389 $\mathrm{gC} \cdot \mathrm{MJ}^{-1}$, but for small-scale areas, it is necessary to consider the differences of ε_{max} among different types of vegetation. Zhu et al. [36] simulated the ε_{max} of various vegetation types based on measured NPP data according to the principle of minimum error. The values of different types of deciduous forests (such as deciduous coniferous forest, deciduous broad-leaved forest, etc.) are similar, which can be merged into one type. The same goes for grassland, cropland, and evergreen forest. In this study, 29 vegetation types in the GLC_FCS30-2020 land cover dataset were reclassified into grassland, cropland, deciduous forest, evergreen forest and others to complete the model calculation.

2.4 Improved disaggregation model for carbon emission distribution

In order to obtain fine resolution carbon emissions, we designed an improved disaggregation method to spatially distribute provincial data into grid level data more reasonably. We use ground transport emissions from the Carbon Monitor China dataset as nonpoint source emissions (*TEmis*) and other sectors as point source emissions (*PEmis*), and spatially disaggregate the two respectively.

For point source emissions, considering the differences in urbanization levels between urban and rural areas, as well as the differences between areas with and without NTL, the study area was divided into three types: lit urban (LU), lit rural (LR), and dark rural (DR) areas. The emissions of each area were calculated separately, and then spatial distribution was performed using NTL data and population grid data according to different weight coefficients.

Urban areas, characterized as centers of human economic activities and primarily built-up regions, contrast with broad rural areas that encompass outer suburbs, vegetation, water bodies, and bare land. In this study, all non-urban regions are classified as rural. The AIEC dataset provides the 10-m LULC classification map of the three UAs (Fig. 1), detailing various land use types. We identified the built-up regions in this dataset as urban areas. For the division between lit and dark areas, we set reasonable thresholds for NTL data to make classification. Unlike most previous studies that used DMSP-OLS with its coarse spatial resolution and high saturation issues in urban areas [25, 27], our analysis employs NPP-VIIRS data, which avoids saturation problems and offers superior data quality [33]. We determined the dark areas by setting a threshold based on the population proportion in these areas, as indicated in previous research [26], finalizing the threshold at around 0.8. Thus, the division of three types of areas was completed.

Furthermore, we used Liu et al.'s method [27] to calculate the $PEmis$ of the three areas. See equation (5) - (9) below:

$$PEmis_{LU} = EPC_U \times SP_{LU} \tag{5}$$

$$PEmis_{LR} = ratio \times EPC_U \times SP_{LR} \tag{6}$$

$$PEmis_{DR} = ratio \times EPC_U \times SP_{DR} \tag{7}$$

$$PEmis = PEmis_{LU} + PEmis_{LR} + PEmis_{DR} \tag{8}$$

$$EPC_U = PEmis/(SP_{LU} + ratio \times SP_{LR} + ratio \times SP_{DR}) \tag{9}$$

where *LU*, *LR*, and *DR* represent lit urban, lit rural and dark rural areas, respectively. $PEmis_{**}$ is the total point source CO_2 emissions of each area, *SP* is the total population of each area, *EPC* is the CO_2 emission per capita, and *ratio* is the EPC ratio in rural area to urban area. $PEmis$ is the total point source CO_2 emissions of the province, and the total population can be obtained through spatial statistics of population grid data. Liu et al. calculated the *ratio* of all provinces of China in 2000, 2005, 2010 and 2013, which showed stable fluctuations without significant changes. We took the four years' average value of each province involved in the three UAs to complete the calculation, and obtained the total $PEmis$ of three types of regions.

Subsequently, we conducted spatial distribution of CO_2 emissions in each region. Liu et al. used NTL data to disaggregate emissions in lit areas and used population grid data to disaggregate emissions in dark rural areas in a linear relationship. Given that both NTL and population factors impact the distribution within all three regions, and their correlations differ, we contemplate employing NTL and population as disaggregation factors for all three regions while assigning different weight coefficients α, β, γ, as follows:

$$PEmis_{LUg} = PEmis_{LU} \times [\alpha \times \frac{L_g}{SL} + (1-\alpha) \times \frac{P_g}{SP}] \tag{10}$$

$$PEmis_{LRg} = PEmis_{LR} \times [\beta \times \frac{L_g}{SL} + (1-\beta) \times \frac{P_g}{SP}] \tag{11}$$

$$PEmis_{DRg} = PEmis_{DR} \times [\gamma \times \frac{L_g}{SL} + (1-\gamma) \times \frac{P_g}{SP}] \tag{12}$$

where g represents the grid level value, L_g and P_g represent the grid values of the NTL and population grid data, respectively. S_L and S_P represent the sum of NTL and population grid values corresponding to the three regions. Another benefit of introducing population weights in lit areas is that it can weaken the impact of extreme NTL values. We used city-level CO_2 emission inventory data as a control standard to determine the optimal weight coefficients to minimize the error in the disaggregating results. Specifically, we disaggregated provincial CO_2 emissions into city-level emissions according to equations (10) to (12), and used the corresponding point-source emissions from the Carbon Monitor Cities-China dataset (CMCC) [1] as the control standard, forming a system of nonhomogeneous linear equations. The coefficient matrix of unknown values (α, β, γ) needs to be preliminarily calculated as grid results, which are then used to derive city-level results through spatial statistics. The optimal α, β, γ are solved using the ordinary least squares method.

For nonpoint source emissions, we referred to Zheng et al.'s method to use road density as weighting factors [39]. The road network density data is derived from OpenStreetMap to calculate the spatial distribution of ground transport emissions (*TEmis*):

$$TEmis_g = TEmis \times \frac{R_g}{SR} \tag{13}$$

where R_g and *SR* represent the grid and sum value of road network density map. Ultimately, the total CO_2 emissions at grid level can be obtained:

$$Emis_g = PEmis_g + TEmis_g \quad (14)$$

2.5 Integrated model for evaluating carbon sinks and sources discrepancies

The net primary productivity *NPP* reflects the net carbon sequestration of vegetation in the urban ecosystem, but still cannot represent the carbon sink of the ecosystem in the region. Instead, the soil heterotrophic respiration R_H should be subtracted to obtain the net ecosystem productivity *NEP*, as shown in Equation (15):

$$NEP = NPP - R_H \quad (15)$$

Soil heterotrophic respiration is related to multiple environmental factors, with temperature and precipitation being the two most important factors [40, 41]. Pei et al. [42] established the relationship between temperature, precipitation and soil respiration based on MODIS data and the measured data at the experimental site, estimated the distribution of soil heterotrophic respiration carbon emissions, as shown in Equation (16):

$$R_H = 0.22 \times (e^{0.0912T} + ln(0.3145PR + 1)) \times 30 \times 46.5\% \quad (16)$$

where *T* represents monthly mean temperature (℃) and *PR* represents monthly total precipitation (mm). Many studies [43-45] applied this model to calculate the NEP distribution in local areas of China, such as Tianjin City and the YRD region, proving that the model is a universal empirical model suitable for forestlands, grasslands, croplands, etc. The monthly temperature and precipitation data of ERA5-Land were used to calculate the soil respiration of the three UAs' ecosystem according to the above equation.

In order to provide data support for the evaluation of carbon neutrality progress, we calculated the following two variables:

$$NCE = Emis - NEP \quad (17)$$

$$pct = NEP/Emis \quad (18)$$

where *Emis* represents the carbon emissions, and *NCE* represents the net carbon emissions of the region to reflect the gap between carbon sources and sinks. *pct* represents the percentage of carbon sinks to carbon emissions. Finally the model calculation of carbon sinks and emissions has been completed, which can further analyze the spatiotemporal discrepancies and policy implications for China's urban carbon neutrality progress.

2.6 Theil index for quantifying the inequality of carbon neutrality

Theil index measures inequality by assessing the uneven distribution of variables based on the entropy principle. Compared to other models used to quantify inequality, the advantage of Theil index is its ability to be subdivided into between-group inequality (T_b) and within-group inequality (T_w), with corresponding contribution rates calculated [9]. The index typically ranges from 0 to 1, where 0 represents complete equality and 1 signifies maximum inequality. To quantify the inequality in NCE distribution within and between cities, this study derived the following equations based on the original model of Theil index and its variant application to carbon emission inequality [9, 46].

$$T_{w,j} = \frac{1}{N}\sum_{i=1}^{N}\left(\frac{NCE_i}{\mu} \times ln\frac{NCE_i}{\mu}\right) \tag{19}$$

$$T_b = \frac{1}{M}\sum_{j=1}^{M}\left(\frac{NCE_j}{\mu_{total}} \times ln\frac{NCE_j}{\mu_{total}}\right) \tag{20}$$

$$T = T_w + T_b = \frac{1}{M}\sum_{j=1}^{M}\left(\frac{NCE_j}{\mu_{total}} \times T_{w,j}\right) + T_b \tag{21}$$

$$R_w = T_w/T, \quad R_b = T_b/T, \quad R_{w,j} = \left(\frac{1}{M} \times \frac{NCE_j}{\mu_{total}} \times T_{w,j}\right)/T \tag{22}$$

Equation (19) calculates the Theil index within city *j*, where *N* is the number of grids in the city, NCE_i is the NCE value of the *i*-th grid, and μ is the average NCE value of all grids in the city. Note that since NCE may have negative values, we adjusted the overall data of a single city by adding the minimum value to all NCE values, ensuring correct calculations. Theil index between cities is calculated as Equation (20), where M is the number of cities in the UA, NCE_j is the average NCE of city j, and μ_{total} is the average NCE of all cities in the UA. The total Theil index T is obtained by the weighted sum of $T_{w,j}$ and T_b . The contribution rate R_w, R_b and $R_{w,j}$ calculated using Equation (22) measure the contribution (%) of T_w, T_b, and $T_{w,j}$ to the total Theil index, indicating the degree to which each component contributes to the overall inequality.

3 Results and discussion

3.1 Precise monitoring of urban carbon dynamics through fine NCE spatiotemporal distribution

Our spatiotemporal distribution results for NCE (Fig. 3) at a 250-m resolution quantified the discrepancies between carbon emissions and sinks, capturing the multiple carbon dynamics that potentially caused the unequal carbon neutrality across the three UAs. Fig. 3a illustrates that high NCE areas are concentrated in urban centers and decrease radially towards surrounding vegetation areas, with the maximum disparity exceeding $420\ \mathrm{gC \cdot m^{-2} \cdot month^{-1}}$. Urban areas consistently exhibit high NCE levels (> $250\ \mathrm{gC \cdot m^{-2} \cdot month^{-1}}$) throughout the year, whereas vegetated areas generally show NCE values around 0 during winter, dropping below -75 $\mathrm{gC \cdot m^{-2} \cdot month^{-1}}$ in summer. The NCE of vegetated areas displays a significant seasonal pattern, decreasing with the latitude of the UA, primarily due to the spatiotemporal dynamics of ecosystem carbon sinks (Fig. S2 & S3). This seasonal trend is also reflected in the monthly average NCE changes of the 10 major cities in Fig. 3c. These high-emission cities maintain positive NCE values throughout the year, indicating substantial carbon sources. However, their NCE values are generally 80-330 $\mathrm{gC \cdot m^{-2} \cdot a^{-1}}$ lower than their carbon emissions (Table 2), highlighting the varying roles of urban green spaces in offsetting carbon emissions.

Specifically, we enlarged representative areas of the three UAs to illustrate cases of carbon dynamics, as shown in Fig. 3b. Urban villages surrounded by highly built areas in Beijing exhibit an NCE of around $100\,\mathrm{gC} \cdot \mathrm{m}^{-2} \cdot \mathrm{month}^{-1}$, significantly lower than the city center (> $300\,\mathrm{gC} \cdot \mathrm{m}^{-2} \cdot \mathrm{month}^{-1}$). In addition, the low NCE effect of urban green parks is even more pronounced, generally below 0. Hangzhou, known for its industrial parks, shows that suburban industrial zones have significantly higher NCE compared to their surroundings. In vegetated areas, the NCE of croplands in Zhaoqing, Guangdong, is almost 80 $\mathrm{gC} \cdot \mathrm{m}^{-2} \cdot \mathrm{month}^{-1}$higher than that of forests, reflecting their weaker carbon sink capacity. These diverse carbon dynamics have led to unequal carbon neutrality effects, while also demonstrating that our NCE results can reveal pronounced intra-urban heterogeneity of urban carbon dynamics.

The observed intra-urban heterogeneity of NCE can be primarily attributed to the following key interrelated drivers. First, industrial structure plays a dominant role, as zones concentrated with heavy industries, manufacturing, and energy-intensive facilities generally exhibit extremely high carbon emissions, leading to elevated NCE. Second, land-use composition strongly differentiates carbon sources and sinks: built-up areas act as persistent carbon sources, while forests, grasslands, and croplands provide effective carbon sinks, creating sharp contrasts within cities. Third, infrastructure distribution, particularly road networks and power plants, contributes to localized emission hotspots, reinforcing spatial heterogeneity in NCE. Together, these drivers shape the uneven carbon neutrality performance observed within and across cities.

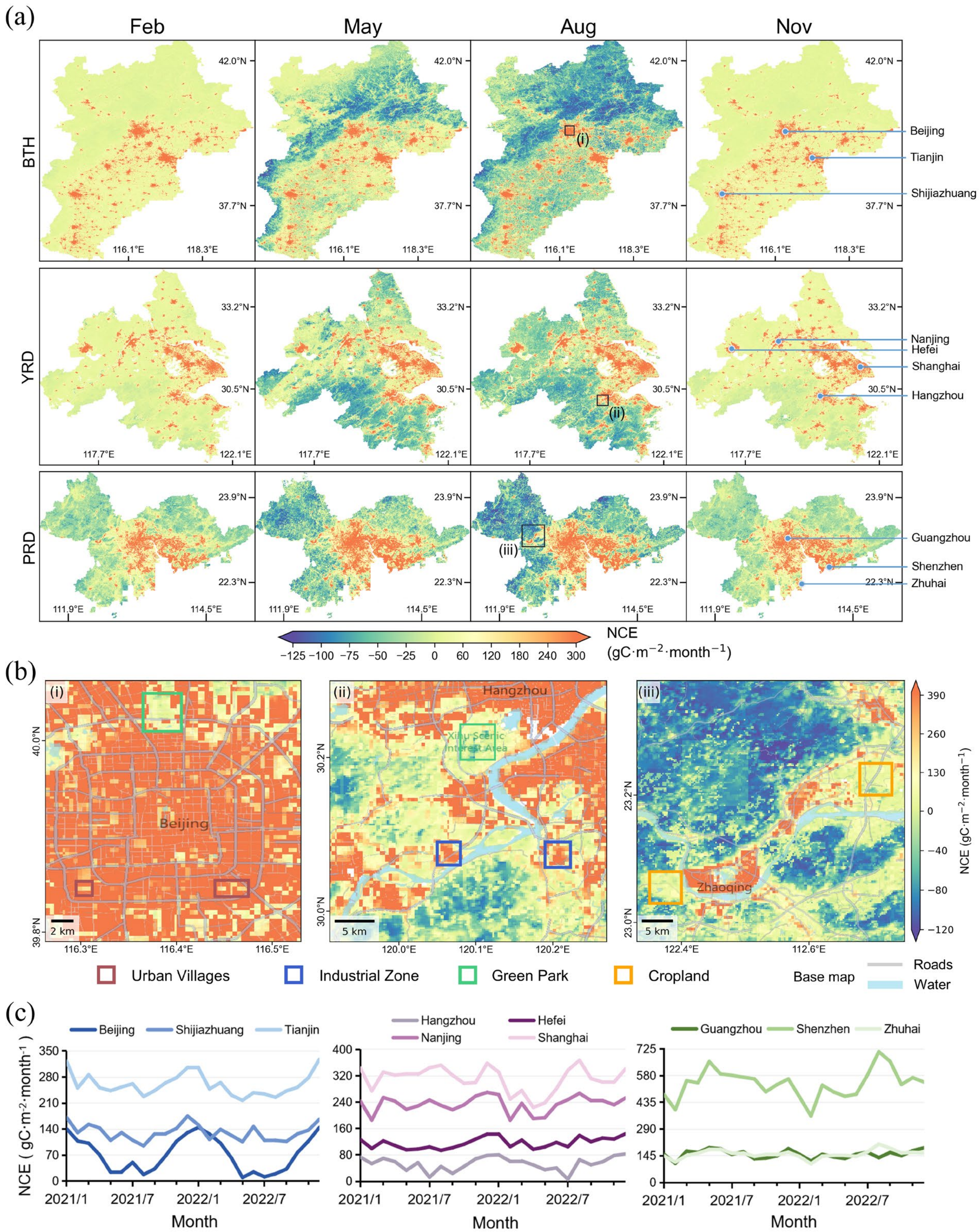
(a)
Feb
May
Aug
Nov
BTH
YRD
PRD
42.0°N
37.7°N
116.1°E
118.3°E
(i)
Beijing
Tianjin
Shijiazhuang
33.2°N
30.5°N
117.7°E
122.1°E
(ii)
Nanjing
Hefei
Shanghai
Hangzhou
23.9°N
22.3°N
111.9°E
114.5°E
(iii)
Guangzhou
Shenzhen
Zhuhai
NCE
(gC·m−2·month−1)
−125 −100 −75 −50 −25 0 60 120 180 240 300
(b)
Beijing
Hangzhou
Zhaoqing
2 km
5 km
Urban Villages
Industrial Zone
Green Park
Cropland
Base map
Roads
Water
NCE (gC·m−2·month−1)
(c)
Beijing
Shijiazhuang
Tianjin
Hangzhou
Hefei
Nanjing
Shanghai
Guangzhou
Shenzhen
Zhuhai
NCE (gC·m-2·month-1)
Month
2021/1
2021/7
2022/1
2022/7

Fig. 3. The three UAs' NCE spatiotemporal distribution (GS 京（2026）2167). **a**, The main quarterly NCE distribution in 2021. When NCE is positive, it indicates carbon source, and vice versa, it indicates carbon sink. The land cover classification map in Fig. 1 helps to identify the urban areas and vegetation areas. **b**, Enlarged maps of urban carbon dynamics. Google Map is used as the base map, and actual landmarks are verified with high-resolution satellite imagery on Google Earth in Fig. S1 to confirm the authenticity of the NCE-captured sites. **c**, The monthly NCE variation of 10 cities. NCE is calculated as the average value within the boundaries of each city.

To further evaluate the reliability and advantages of our results, we compared the NPP and carbon emission results used to generate NCE with similar datasets. We conducted correlation analyses between MODIS NPP data product (MOD17A3HGF) [47] and the CASA model NPP results, as well as between Open-source Data Inventory for Anthropogenic CO_2 (ODIAC) product [48] and our disaggregation emission results, as shown in Fig. S5. Our NPP results showed a significant correlation with the MODIS data, with a Pearson correlation coefficient (R) of 0.66 and a root mean square error (RMSE) of 206. Similarly, our disaggregated emission results correlated well with the ODIAC products (R = 0.79, RMSE = 1665). These comparisons indicate that the differences between the datasets are relatively small, affirming the high credibility of our results. The specific uncertainty analysis is discussed in Sect. 3.5.

Additionally, we selected a small area around Hangzhou City in YRD for magnification to more clearly display the differences at fine scale, as shown in Fig. 4. Due to data quality issues, MODIS NPP in urban areas was neglected. In contrast, CASA NPP provided better data quality and more spatial variation details. For carbon emission data, our results also showed good spatial heterogeneity at the urban scale compared to the ODIAC product, such as the distribution of precise point source emissions and traffic line source emissions. This granularity supports the characterization of urban carbon dynamics and can accurately quantify the discrepancies between carbon emissions and sinks at a small scale for urban carbon neutrality process.

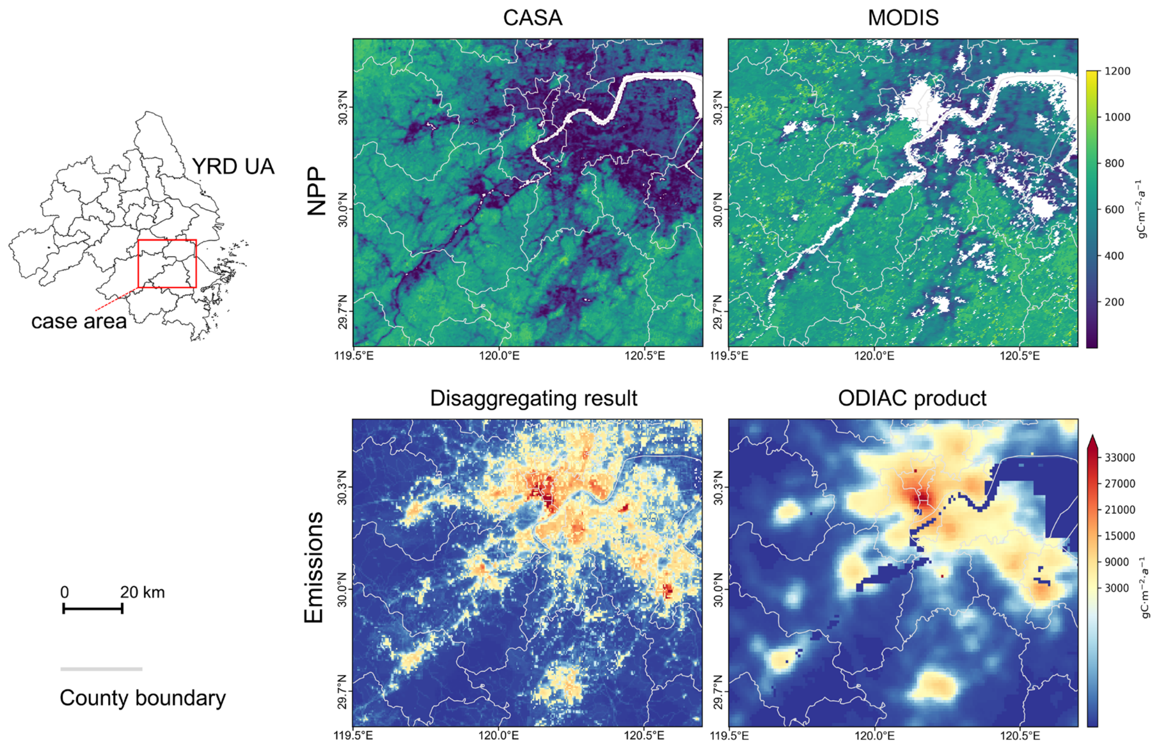

Fig. 4. Comparison between this study's results and similar products. Case area was selected around Hangzhou City, and the complete NPP and emission results of the three UAs are shown in Fig. S2 & S4 (GS 京（2026）2167).

3.2 Evaluation of the carbon neutrality process below the city level

The evaluation of the carbon neutrality process for all cities in the three UAs indicates that only 5 out of 48 cities function as carbon sinks, while the remaining cities demonstrate different level of carbon sources. We computed the annual average and total amounts of NPP, NEP, Emission and NCE for all cities (Table 2, Tables S1-S3), and determined the percentage of carbon sinks to carbon emissions (*pct*) of each city in Fig. S6. The statistics show that 23 cities have *pct* values less than 13.6%, the estimated percentage of carbon sinks offsetting emissions when China reaches the 2030 carbon peak under management policy intervention [49]. These cities tend to be heavily industrialized or densely populated metropolises, all with NCE values exceeding 1000 $gC \cdot m^{-2} \cdot a^{-1}$. In contrast, resource-oriented or tourism-oriented cities, such as Zhaoqing (321%) and Chengde (165%), have already achieved carbon neutrality and become significant carbon absorbers. Among the 10 major cities analyzed, Hangzhou (29.2%) and Beijing (23.6%) ranked the highest, with the remaining cities all below 15%, reflecting prevalent high emissions and low sinks in the UAs. The *pct* for the three UAs ranges from 13% to 32%, indicating a significant gap between China's major UAs and the achievement of carbon neutrality.

Given the finer resolution of our results, there is potential to explore carbon source and sink characteristics at sub-urban levels, such as counties. This provides crucial support for detailed regional carbon reduction action plans. For cities and counties that have reached or are close to carbon neutrality, continuous monitoring of their carbon sequestration capabilities is necessary, along with the exploration of sustainable development strategies to maintain this status. For those far from carbon neutrality, it is essential to formulate stricter carbon reduction plans and enhance urban greening to increase their carbon sink capacity. Specific policy measures can be inspired by the fine carbon sink and emission maps that we generated, as discussed later in Sect. 3.4.

Table 2. Annual results of NPP, NEP, Emission, NCE and pct of 25 cities.

Province	City	Annual average ($gC \cdot m^{-2} \cdot a^{-1}$)				Annual total amount ($Kt\ C \cdot a^{-1}$)				pct
		NPP	NEP	Emission	NCE	NPP	NEP	Emission	NCE	(%)
Beijing	Beijing	444.9	269.3	1138.9	869.6	7332.3	4438.2	18770.3	14332.1	23.6
Tianjin	Tianjin	295.8	82.5	3207.9	3125.4	3490.6	974.1	37859.0	36884.9	2.6
Hebei	Chengde	452.3	328.8	199.3	**-129.5**	18257.0	13270.2	8043.3	**-5226.9**	**165.0**

	Qinhuangdao	427.7	256.9	1086.4	829.5	3345.7	2009.7	8498.9	6489.2	23.6
	Shijiazhuang	418.4	209.0	1783.0	1574.1	5741.6	2867.6	24469.1	21601.5	11.7
	Xingtai	390.0	164.6	1151.0	986.3	4679.0	1975.5	13809.9	11834.4	14.3
	Zhangjiakou	282.9	166.2	312.4	146.2	10560.5	6204.6	11663.7	5459.1	53.2
Shanghai	Shanghai	267.4	-9.5	3716.9	3726.5	1695.6	-60.4	23565.3	23625.8	-0.3
Anhui	Anqing	524.0	251.7	380.4	128.8	6985.7	3355.6	5072.2	1716.6	66.2
	Chizhou	593.2	313.8	201.0	**-112.8**	4908.8	2597.0	1663.7	**-933.3**	**156.1**
	Hefei	376.7	98.6	1496.2	1397.5	4302.1	1126.5	17086.0	15959.5	6.6
	Ma’anshan	397.3	119.2	874.5	755.3	1612.1	483.7	3548.3	3064.6	13.6
	Xuancheng	591.8	324.3	266.2	**-58.1**	7202.2	3947.3	3240.1	**-707.3**	**121.8**
Jiangsu	Nanjing	363.7	92.2	2901.4	2809.1	2398.9	608.4	19136.4	18527.9	3.2
	Wuxi	319.3	37.3	3545.4	3508.2	1472.4	171.9	16350.5	16178.6	1.1
	Yancheng	378.4	129.5	685.7	556.1	5980.4	2047.4	10836.8	8789.4	18.9
	Yangzhou	366.5	104.1	1201.2	1097.2	2438.5	692.4	7992.5	7300.1	8.7
Zhejiang	Hangzhou	540.4	265.4	909.8	644.5	8928.7	4384.4	15033.1	10648.7	29.2
	Ningbo	425.7	143.1	1635.4	1492.3	3989.0	1340.7	15325.1	13984.4	8.7
	Zhoushan	475.4	194.6	1165.9	971.3	644.1	263.6	1579.7	1316.1	16.7
Guangdong	Guangzhou	691.2	326.1	2165.2	1839.2	5063.9	2388.9	15863.4	13474.5	15.1
	Jiangmen	858.7	485.0	470.7	**-14.2**	8109.0	4579.8	4445.3	**-134.5**	**103.0**
	Shenzhen	607.7	229.1	6679.3	6450.2	1196.1	450.9	13145.2	12694.3	3.4
	Zhaoqing	980.4	637.5	198.9	**-438.6**	14854.3	9658.9	3014.0	**-6644.9**	**320.5**
	Zhuhai	484.9	89.3	1944.9	1855.6	774.3	142.6	3105.7	2963.1	4.6

This table compiles 25 cities at different *pct* levels, with complete inventories for all cities presented in Tables S1-S3. *pct* exceeding 100% signifies carbon neutrality. The city location can be found in Fig. 1.

3.3 Unequal contributions to carbon neutrality between and within cities

The between- and within-city Theil indices reveal varying degrees of inequality in contributions to carbon neutrality among the three UAs (Fig. 5). This study is the first to calculate grid-level Theil index within a city ($T_{w,j}$), enabled by high-resolution NCE data, providing a detailed understanding of the spatial structure of carbon neutrality in the inner city. Cities with higher $T_{w,j}$ values, represented by lighter colors, indicate highly uneven NCE distributions, potentially driven by a few emission-intensive zones that create significant disparities in urban carbon source-sink dynamics. High-$T_{w,j}$ cities ($T_{w,j}$ >0.11) in BTH and PRD generally align with low *pct* cities (Fig. S6). However, the highest $T_{w,j}$ in YRD appeared in Ma'anshan and its surrounding cities, rather than Shanghai. The Hefei-Chuzhou-Ma'anshan region is an industrial city cluster in Anhui Province, home to heavy industrial sources such as chemical plants, non-ferrous metal smelters, and steel plants. Ma'anshan's $T_{w,j}$ exceeds 0.2, ranking the highest among the three UAs. As a major industrial city renowned for its extensive steel industry, Ma'anshan exhibits concentrated carbon emissions from steel plants, leading to significant carbon neutrality inequalities. In contrast, resource-based and tourism-oriented cities, characterized by more evenly distributed green spaces that reduce carbon emission inequalities, exhibit lower $T_{w,j}$ values (<0.07), generally corresponding with high *pct* cities. The size of the circles on each city reflects its contribution rate ($R_{w,j}$) to the total Theil index T, which is calculated based on the city's $T_{w,j}$ and its NCE weight in the total NCE (see Methods). Although Ma'anshan has a high $T_{w,j}$ value, its contribution rate is lower than that of Shanghai. This is attributed to Shanghai's annual mean NCE of 3726.5 $\mathrm{gC \cdot m^{-2} \cdot a^{-1}}$, significantly higher than Ma'anshan's 755.3 $\mathrm{gC \cdot m^{-2} \cdot a^{-1}}$ (Table 2), resulting in a greater weight. In general, high-NCE cities play a dominant role in shaping the carbon neutrality inequality of the entire urban agglomeration.

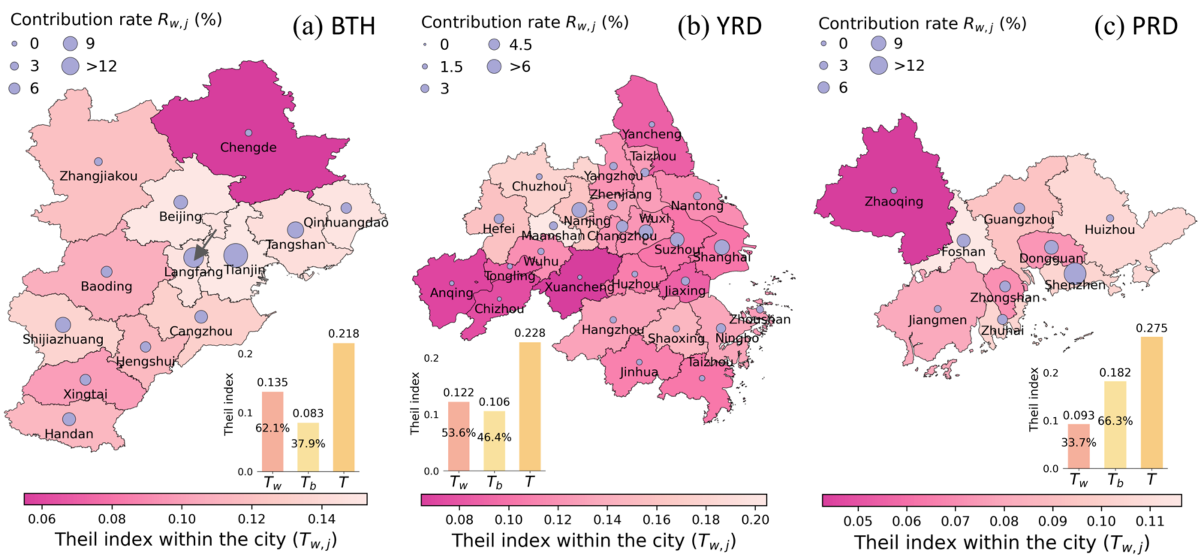

Fig. 5. Theil indices and contribution rates between and within cities of the three UAs. The index ranges from 0 to 1, with larger values indicating greater inequality. The percentage on the bar chart represents the corresponding contribution rate (R_w, R_b) of T_w and T_b to total Theil index T (GS 京（2026）2167).

Overall, the T_w values and their contributions to T follow a decreasing trend of “BTH > YRD > PRD”, while T_b exhibits the opposite trend. The gradual decline in T_w indicates that the NCE distribution within cities is becoming more balanced. This trend can be attributed to the optimization of internal industrial structures or the regionally equitable implementation of emission reduction policies. For BTH, the relatively high T_w suggests significant inequalities in intra-city NCE distributions. These inequalities may be driven by emission-intensive industrial infrastructures or uneven energy consumption patterns. In contrast, PRD’s lower T_w reflects smaller intra-city NCE disparities, likely indicative of a more balanced industrial distribution and relatively even urban green space coverage.

The increasing T_b across the three UAs suggests that inter-city NCE disparities are widening. This trend reflects imbalances in industrial layouts between core cities and peripheral cities within urban agglomerations. PRD's higher T_b indicates pronounced differences in economic and industrial development models within the region. For instance, the Bay Area centered around Shenzhen may exhibit significantly higher emission intensity than surrounding cities due to the high proportion of high-tech industries. In contrast, BTH's lower T_b suggests a more uniform NCE pattern across cities, potentially resulting from the dominance of traditional industries in the region.

These findings highlight substantial differences in industrial distribution and policy implementation across the three major UAs. The analysis demonstrates that a comprehensive assessment, integrating the city's overall NCE level, the between- and within-city Theil index, and its contribution rate to regional inequality, is crucial for obtaining accurate and holistic insights. This integrated metric framework indicates that urban carbon management must leverage such a multi-dimensional diagnosis to effectively guide policy. Future regional coordination policies should take into account the unique characteristics of each city, with a focus on reducing both intra- and inter-city inequalities to promote greater fairness and synergy in contributions to carbon neutrality.

3.4 Policy implications for reducing inequalities in carbon neutrality contributions

Cities with high $T_{w,j}$ and high $R_{w,j}$ are key areas requiring targeted policy interventions. These cities can benefit from valuable guidance for urban afforestation and emission reduction strategies aimed at mitigating carbon neutrality inequalities. The potential of urban vegetation in offsetting anthropogenic carbon emissions can be fully explored with fine-resolution carbon sink characteristics. By combining the potential forestation map provided by Xu et al. [50]

(https://doi.org/10.5281/zenodo.8297679) with our NEP results (Fig. S3), new policy recommendations for urban green space transformation can be developed. We took Beijing as an example to calculate the distribution of NEP at different levels, as shown in Fig. 6a&b. Nearly half the region exhibits an annual average NEP exceeding 300 $gC \cdot m^{-2} \cdot a^{-1}$, which suggests a young forest age with significant potential for increased carbon sinks [50]. We plotted potential forestation areas (grey) in Fig. 6a, treating areas with NEP below 300 $gC \cdot m^{-2} \cdot a^{-1}$ as low NEP areas suitable for renovation. We also distinguished forest, cropland, grass and shrub based on land-use and land-cover (LULC) types (Fig. 6a&c). More than 700 km^2 of forests and cropland in Beijing were found to have transformation opportunities. Low NEP forest areas may indicate a decrease in carbon sequestration capacity due to aging or disturbances; therefore, optimizing forest age structure can enhance the region's carbon sink potential [51]. Given the geographical advantages, cropland, grass, and shrub areas can consider reforestation or implementing a suitable spatial layout to introduce appropriate tree species, forming a composite vegetation system to achieve ecological synergy. This analysis can be applied to other cities as well. Practical applications should integrate afforestation plans with regional development strategies, balancing ecological, social, and economic impacts to ensure more equitable contributions to carbon neutrality.

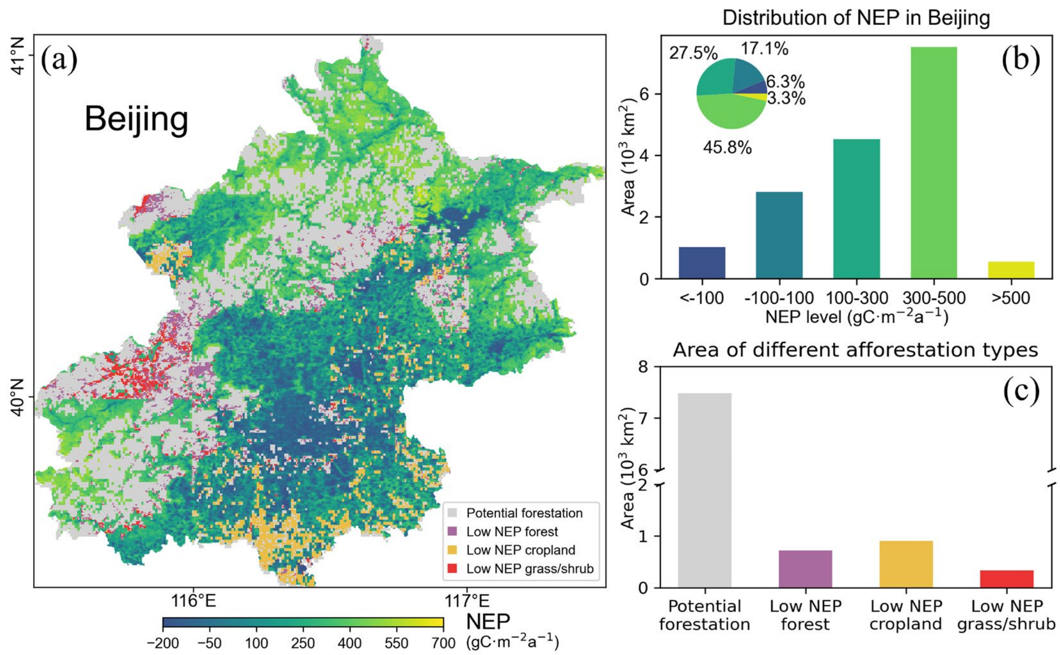

Fig. 6. Distribution of potential forestation areas in Beijing (GS 京（2026）2167). **a**, Distribution of NEP and potential forestation areas. The high-confidence potential forestation map (grey) for China at a 1km resolution was generated by Xu et al. [50] using dynamic global vegetation models and machine learning methods to provide guidance for the key issue of "where is suitable to afforest" for carbon neutrality goals. **b,c**, Area statistics of NEP (**b**) and afforestation types (**c**).

For emission reduction, the improved spatial distribution of carbon emissions (Fig. S4) enables precise identification and quantification of emission hotspots to formulate targeted policies. Notably, identifying regions with disproportionately high emissions, such as Tangshan and Tianjin, where emissions exceed 25,000 $\mathrm{Kt\,C \cdot a^{-1}}$, allows for the enactment of tailored regulatory measures, including stringent emission standards or incentives for green technology adoption suited to local conditions. The high-resolution emission distribution map delineates areas of intense carbon emissions from both point and nonpoint sources in urban and rural settings. This enables decision-makers to implement targeted interventions, such as prioritizing renewable energy in high-emission suburban industrial parks or enhancing public transportation systems to curtail vehicle emissions.

Additionally, the Theil index analysis provides a critical quantitative foundation for optimizing carbon market mechanisms and implementing differentiated carbon quota allocation policies. Our findings, which dissect carbon neutrality inequalities both within and between cities, enable a multi-tiered allocation strategy. At the inter-city level, the quantified inequality can guide the initial distribution of city-level emission budgets, ensuring that cities with historically lower cumulative emissions and greater carbon sink contributions are not unfairly burdened, thereby addressing historical responsibilities and ecological contributions. More critically, the intra-city inequality supports a finer-grained allocation within a city’s jurisdiction. Urban administrators can use this to set differentiated targets for distinct districts or industrial sectors. For example, districts identified with high NCE would receive stricter reduction quotas, directly linking quota pressure to the spatial patterns of carbon imbalance. Conversely, districts with significant carbon sink capacity could be allocated less stringent emission quotas or receive economic compensation for their ecosystem services, incentivizing the preservation and expansion of urban green spaces. This approach ensures that carbon quota allocation can effectively incentivize different regions and industries to reduce emissions based on their unique circumstances. Through this differentiated quota allocation, the coordination between economic development and environmental protection can be promoted more fairly, achieving carbon emission reduction while mitigating regional carbon neutrality inequality.

3.5 Uncertainties and limitations

Although we evaluated and validated the results of our model calculations, some uncertainties and limitations remain in this study. The accuracy of the CASA model and soil respiration model is influenced by the input remote sensing and meteorological data, potentially leading to deviations from true values. Previous studies have validated the CASA model results against field-measured NPP, showing R^2 values ranging from 0.73 to 0.82 [17, 52]. This demonstrates good consistency between the NPP calculated by the CASA model and observed NPP. However, due to our extensive research area, we were unable to obtain sufficient field observations for carbon sink validation. Therefore, we only compared and validated NPP with authoritative MODIS products. Additionally, we used NEP as the carbon sink indicator and did not account for natural disturbances such as wildfires and insect infestations, which may also contribute to deviations in carbon sink estimates.

The uncertainty of grid-level carbon emissions primarily arises from total provincial emissions and spatial disaggregation methods. The provincial emission data that we used employed a set of sectoral activity data and corresponding emission factors to calculate emissions from multiple sectors according to IPCC Guidelines, with an overall uncertainty of ± 7.2% [53]. The overall uncertainty of grid-level data we obtained should not exceed this range. However, for specific grid points, there may be additional overestimation or underestimation due to the uncertainty of disaggregation methods. Our improved method makes spatial distribution more reasonable by considering the heterogeneity of emission intensity between urban and rural areas, as well as different allocation methods for point and nonpoint source emissions, achieving unprecedented resolution. The comparative analysis demonstrates that our refined results still have good reliability. Therefore, by integrating the results of carbon sinks and emissions and quantifying the discrepancies, we can reasonably evaluate the urban carbon neutrality process and obtain valuable policy implications.

It should be noted that the estimated NCE and related inequality results in this study reflect regional carbon balance from a production perspective. The provincial anthropogenic CO_2 emission data used in this study are obtained from the Carbon Monitor China dataset, which estimates production-based emissions under the territorial accounting principle. Production-based accounting quantifies emissions that physically occur within a regional boundary, covering fossil fuel combustion and industrial processes. By contrast, consumption-based (responsibility-based) accounting further incorporates emission outsourcing, cross-regional consumption transfer, and carbon embodied in interregional trade, which reallocate emission responsibilities to regions where products are finally consumed rather than produced [54]. These aspects should be considered when interpreting regional contributions to carbon neutrality from a responsibility-based viewpoint.

4 Conclusion

In this study, we developed an integrated model to quantify the contributions of carbon neutrality within Chinese cities. We performed model calculations for ecosystem carbon sinks and the distribution of anthropogenic carbon emissions across three urban agglomerations in China, thus obtaining the 250-m spatiotemporal variations in NCE. Compared with existing studies on urban carbon emissions and carbon neutrality, our framework delivers three key advances: (i) a robust integrated model that couples ecosystem carbon sinks and human-induced carbon emissions; (ii) unprecedented fine spatiotemporal details that capture fine-scale urban carbon heterogeneity; and (iii) the explicit grid-level quantification of intra-urban carbon neutrality inequality using the Theil index. Validations against existing datasets confirm the reliability of our results. The refined depiction of urban carbon dynamics enables a rigorous and spatially explicit evaluation of carbon neutrality progress and its unequal distribution within and across cities. These findings provide targeted and actionable insights for urban afforestation, high-emission sector mitigation, and spatially differentiated policy interventions.

The outcomes of this study were driven by multi-source remote sensing data to obtain a 250-m urban NCE distribution. Data of new generation satellites (e.g., Landsat8 at 30-m resolution) can provide even more detailed indices for use in the model, demonstrating huge potential for further applications to derive NCE for smaller-scale areas. The results of this study can also be used to derive county-level inventories and fill gaps in county-level carbon emission and sink data in China, facilitating the investigation of county-level contributions to carbon neutrality.

Given that the study area encompasses urban and rural areas with a certain population density, as well as various vegetation areas such as forests, grasslands and croplands, it better demonstrates the dynamics of urban carbon sinks and emissions with good typicality and representativeness. Although we focus on three highly developed eastern urban agglomerations (BTH, YRD, PRD), the proposed framework is equally applicable to cities in central and western China, which generally feature relatively lower development levels but considerable carbon sink capacity and growing importance in national carbon neutrality strategy. Because the identical data sources are publicly accessible, the calculation of NCE can be extended to any other city in China, which is highly significant for quantifying the carbon neutrality levels and contributions across a broader scope. This extensibility enables consistent carbon mapping and inequality assessment for both eastern high-emission regions and central/western carbon sink–rich regions, supporting coordinated and regionally differentiated policy formulation. It also offers valuable insights for guiding urbanization development and the establishment of low-carbon cities, ultimately supporting the long-term goals of carbon neutrality in China.

Acknowledgements

None.

Author contribution statement

L.W.: methodology, data collection, analysis and visualization, writing-original draft. Z.S.: conceptualization, methodology. T.S. and T.L.: writing-review and editing.

Data availability

The data that support the findings of this study are available from the corresponding author upon reasonable request.

Declaration of competing interest

All the contributing authors report no conflict of interests in this work.

Funding

None.

Use of AI statement

None.

Supplementary material

Supplementary material including Text S1-S2, Tables S1-S3 and Figures S1-S6 is available in the online version of this article at https://doi.org/10.26599/CS.2026.9510010.

References

[1]Huo D, Liu K, Liu J, Huang Y, Sun T, Sun Y, Si C, Liu J, Huang X, Qiu J, et al. Near-real-time daily estimates of fossil fuel CO_2 emissions from major high-emission cities in China. *Scientific Data*. 2022; 9(1): 684.

[2]Duan L, Liu Z, Wen Y, Chen W, Jin D, Sun S and Dai R. Trend of Urbanization Rate in China Various Regions. *IOP Conference Series: Earth and Environmental Science*. 2021; 772: 012008.

[3]Bemis G and Allen J. Inventory of California greenhouse gas emissions and sinks: 1990 to 2002 update. *California Energy Commission. CEC-600-2005-025*. 2005.

[4]Zhang W, Huang B and Luo D. Effects of land use and transportation on carbon sources and carbon sinks: A case study in Shenzhen, China. *Landscape and Urban Planning*. 2014; 122: 175–185.

[5]Xia M, Chuai X, Zhai L, Xiang A and Wang T. High-resolution carbon neutrality mapping and a heterogeneity analysis for China's two typical megalopolises. *Urban Climate*. 2023; 49: 101488.

[6]Piao S, Yue C, Ding J and Guo Z. Perspectives on the role of terrestrial ecosystems in the 'carbon neutrality' strategy. *Science China-Earth Sciences*. 2022; 65(6): 1178–1186.

[7]Xia X, Ren P, Wang X, Liu D, Chen X, Dan L, He B, He H, Ju W, Liang M, et al. The carbon budget of China: 1980-2021. *Science Bulletin*. 2024; 69(1): 114–124.

[8]Clarke-Sather A, Qu J, Wang Q, Zeng J and Li Y. Carbon inequality at the sub-national scale: A case study of provincial-level inequality in CO_2 emissions in China 1997-2007. *Energy Policy*. 2011; 39(9): 5420–5428.

[9]Cui Y, Khan S U, Deng Y and Zhao M. Spatiotemporal heterogeneity, convergence and its impact factors: Perspective of carbon emission intensity and carbon emission per capita considering carbon sink effect. *Environmental Impact Assessment Review*. 2022; 92: 106699.

[10]Xu C. Determinants of carbon inequality in China from static and dynamic perspectives. *Journal of Cleaner Production*. 2020; 277: 123286.

[11]Fernandez-Martinez M, Sardans J, Chevallier F, Ciais P, Obersteiner M, Vicca S, Canadell J G, Bastos A, Friedlingstein P, Sitch S, et al. Global trends in carbon sinks and their relationships with CO_2 and temperature. *Nature Climate Change*. 2019; 9(1): 73–+.

[12]Piao S, He Y, Wang X and Chen F. Estimation of China’s terrestrial ecosystem carbon sink: Methods, progress and prospects. *Science China Earth Sciences*. 2022; 65(4): 641–651.

[13]Zenbei U and Hiroshi S. Agroclimatic Evaluation of Net Primary Productivity of Natural Vegetations. *Journal of Agricultural Meteorology*. 1985; 40(4): 343–352.

[14]Landsberg J J and Waring R H. A generalised model of forest productivity using simplified concepts of radiation-use efficiency, carbon balance and partitioning. *Forest Ecology and Management*. 1997; 95(3): 209–228.

[15]Potter C S, Randerson J T, Field C B, Matson P A, Vitousek P M, Mooney H A and Klooster S A. Terrestrial ecosystem production: A process model based on global satellite and surface data. *Global Biogeochemical Cycles*. 1993; 7(4): 811–841.

[16]Schaefer K, Collatz G J, Tans P, Denning A S, Baker I, Berry J, Prihodko L, Suits N and Philpott A. Combined Simple Biosphere/Carnegie-Ames-Stanford Approach terrestrial carbon cycle model. *Journal of Geophysical Research-Biogeosciences*. 2008; 113(G3): G03034.

[17]Liang W, Yang Y, Fan D, Guan H, Zhang T, Long D, Zhou Y and Bai D. Analysis of spatial and temporal patterns of net primary production and their climate controls in China from 1982 to 2010. *Agricultural and Forest Meteorology*. 2015; 204: 22–36.

[18]Bao G, Bao Y, Qin Z, Xin X, Bao Y, Bayarsaikan S, Zhou Y and Chuntai B. Modeling net primary productivity of terrestrial ecosystems in the semi-arid climate of the Mongolian Plateau using LSWI-based CASA ecosystem model. *International Journal of Applied Earth Observation and Geoinformation*. 2016; 46: 84–93.

[19]Li M, Liu H, Geng G, Hong C, Liu F, Song Y, Tong D, Zheng B, Cui H, Man H, et al. Anthropogenic emission inventories in China: a review. *National Science Review*. 2017; 4(6): 834–866.

[20]Shan Y, Guan D, Zheng H, Ou J, Li Y, Meng J, Mi Z, Liu Z and Zhang Q. Data Descriptor: China CO_2 emission accounts 1997-2015. *Scientific Data*. 2018; 5: 170201.

[21]Zheng B, Tong D, Li M, Liu F, Hong C, Geng G, Li H, Li X, Peng L, Qi J, et al. Trends in China's anthropogenic emissions since 2010 as the consequence of clean air actions. *Atmospheric Chemistry and Physics*. 2018; 18(19): 14095–14111.

[22]Doll C N H, Muller J P and Elvidge C D. Night-time imagery as a tool for global mapping of socioeconomic parameters and greenhouse gas emissions. *Ambio*. 2000; 29(3): 157–162.

[23]Ghosh T, Elvidge C D, Sutton P C, Baugh K E, Ziskin D and Tuttle B T. Creating a Global Grid of Distributed Fossil Fuel CO_2 Emissions from Nighttime Satellite Imagery. *Energies*. 2010; 3(12): 1895–1913.

[24]Su Y, Chen X, Li Y, Liao J, Ye Y, Zhang H, Huang N and Kuang Y. China's 19-year city-level carbon emissions of energy consumptions, driving forces and regionalized mitigation guidelines. *Renewable & Sustainable Energy Reviews*. 2014; 35: 231–243.

[25]Cui X, Lei Y, Zhang F, Zhang X and Wu F. Mapping spatiotemporal variations of CO_2 (carbon dioxide) emissions using nighttime light data in Guangdong Province. *Physics and Chemistry of the Earth*. 2019; 110: 89–98.

[26]Elvidge C D, Baugh K E, Sutton P C, Bhaduri B and Erwin E H. Who's in the Dark—Satellite Based Estimates of Electrification Rates. Urban Remote Sensing: Monitoring, Synthesis and Modeling in the Urban Environment; 2011.

[27]Liu X, Ou J, Wang S, Li X, Yan Y, Jiao L and Liu Y. Estimating spatiotemporal variations of city-level energy-related CO_2 emissions: An improved disaggregating model based on vegetation adjusted nighttime light data. *Journal of Cleaner Production*. 2018; 177: 101–114.

[28]Liu S, Wang H, Hu Y, Zhang M, Zhu Y, Wang Z, Li D, Yang M and Wang F. Land Use and Land Cover Mapping in China Using Multimodal Fine-Grained Dual Network. *IEEE Transactions on Geoscience and Remote Sensing*. 2023; 61: 1–19.

[29]Shen S, Wu C, Gai Z and Fan C. Analysis of the Spatiotemporal Evolution of the Net Carbon Sink Efficiency and Its Influencing Factors at the City Level in Three Major Urban Agglomerations in China. *Int J Environ Res Public Health*. 2023; 20(2).

[30]Munoz-Sabater J, Dutra E, Agusti-Panareda A, Albergel C, Arduini G, Balsamo G, Boussetta S, Choulga M, Harrigan S, Hersbach H, et al. ERA5-Land: a state-of-the-art global reanalysis dataset for land applications. *Earth System Science Data*. 2021; 13(9): 4349–4383.

[31]Didan K. MODIS/Terra Vegetation Indices 16-Day L3 Global 250m SIN Grid V061 [Dataset]. 2021. https://doi.org/10.5067/MODIS/MOD13Q1.061

[32]Zhang X, Liu L, Chen X, Gao Y, Xie S and Mi J. GLC_FCS30: global land-cover product with fine classification system at 30m using time-series Landsat imagery. *Earth System Science Data*. 2021; 13(6): 2753–2776.

[33]Elvidge C D, Baugh K E, Zhizhin M and Hsu F C. Why VIIRS data are superior to DMSP for mapping nighttime lights. *Proceedings of the Asia Pacific Advanced Network*. 2013; 35.

[34]Elvidge C D, Baugh K, Zhizhin M, Hsu F C and Ghosh T. VIIRS night-time lights. *International Journal of Remote Sensing*. 2017; 38(21): 5860–5879.

[35]CIESIN. Gridded Population of the World, Version 4 (GPWv4): Population Density, Revision 11 [Dataset]. 2018. http://dx.doi.org/10.7927/H49C6VHW

[36]Zhu W, Pan Y and Zhang J. Estimation of net primary productivity of chinese terrestrial vegetation based on remote sensing. *Zhiwu Shengtai Xuebao*. 2007; 31(3): 413–424.

[37]Meraj G, Kanga S, Ambadkar A, Kumar P, Singh S K, Farooq M, Johnson B A, Rai A and Sahu N. Assessing the Yield of Wheat Using Satellite Remote Sensing-Based Machine Learning Algorithms and Simulation Modeling. *Remote Sensing*. 2022; 14(13): 3005.

[38]Piao S, Fang J and Guo Q. Application of CASA model to the estimation of Chinese terrestrial net primary productivity. *Acta Phytoecologica Sinica*. 2001; 025(005): 603–608. https://www.plant-ecology.com/EN/Y2001/V25/I5/603

[39]Zheng B, Huo H, Zhang Q, Yao Z L, Wang X T, Yang X F, Liu H and He K B. High-resolution mapping of vehicle emissions in China in 2008. *Atmospheric Chemistry and Physics*. 2014; 14(18): 9787–9805.

[40]Flanagan L B, Sharp E J and Letts M G. Response of plant biomass and soil respiration to experimental warming and precipitation manipulation in a Northern Great Plains grassland. *Agricultural and Forest Meteorology*. 2013; 173: 40–52.

[41]Bond-Lamberty B and Thomson A. Temperature-associated increases in the global soil respiration record. *Nature*. 2010; 464(7288): 579–U132.

[42]Pei Z, Zhou C, Ouyang H and Yang W. A carbon budget of alpine steppe area in the Tibetan Plateau. *Geographical Research*. 2010; 29(1): 102–110. https://www.dlyj.ac.cn/CN/10.11821/yj2010010010

[43]Cao S, Yi H, Zhang L, Sun Q, Zhang Y, Li H, Wei X and Liu Y. Spatiotemporal dynamics of vegetation net ecosystem productivity and its response to drought in Northwest China. *Giscience & Remote Sensing*. 2023; 60(1): 2194597.

[44]Ling S, Gao Z, Ma C and You H. Estimation of net primary productivity of vegetation and vegetation carbon sink in Tianjin area based on CASA model. *Tianjin Agricultural Sciences*. 2022; 28(12): 69–75+81.

[45]Zou C, Li H, Chen D, Fan J, Liu Z, Xu X, Li J and Wang Z. Spatial-Temporal Changes of Carbon Source/Sink in Terrestrial Vegetation Ecosystem and Response to Meteorological Factors in Yangtze River Delta Region (China). *Sustainability*. 2022; 14(16).

[46]Theil H. Economics and information theory. 1967.

[47]Running S, Zhao, M. MOD17A3HGF MODIS/Terra Net Primary Production Gap-Filled Yearly L4 Global 500 m SIN Grid V006 [Dataset]. 2019. HTTPS://DOI.ORG/10.5067/MODIS/MOD17A3HGF.006

[48]Oda T, Maksyutov S and Andres R J. The Open-source Data Inventory for Anthropogenic CO_2, version 2016 (ODIAC2016): a global monthly fossil fuel CO_2 gridded emissions data product for tracer transport simulations and surface flux inversions. *Earth System Science Data*. 2018; 10(1): 87–107.

[49]Huang Y, Sun W, Qin Z, Zhang W, Yu Y, Li T, Zhang Q, Wang G, Yu L, Wang Y, et al. The role of China's terrestrial carbon sequestration 2010-2060 in offsetting energy-related CO_2 emissions. *National Science Review*. 2022; 9(8).

[50]Xu H, Yue C, Zhang Y, Liu D and Piao S. Forestation at the right time with the right species can generate persistent carbon benefits in China. *Proceedings of the National Academy of Sciences of the United States of America*. 2023; 120(41): e2304988120.

[51]Besnard S, Carvalhais N, Arain M A, Black A, de Bruin S, Buchmann N, Cescatti A, Chen J, Clevers J G P W, Desai A R, et al. Quantifying the effect of forest age in annual net forest carbon balance. *Environmental Research Letters*. 2018; 13(12): 124018.

[52]Jay S, Potter C, Crabtree R, Genovese V, Weiss D J and Kraft M. Evaluation of modelled net primary production using MODIS and landsat satellite data fusion. *Carbon Balance and Management*. 2016; 11: 8.

[53]Liu Z, Ciais P, Deng Z, Davis S J, Zheng B, Wang Y, Cui D, Zhu B, Dou X, Ke P, et al. Carbon Monitor, a near-real-time daily dataset of global CO_2 emission from fossil fuel and cement production. *Scientific Data*. 2020; 7(1): 392.

[54]Xing Z, Ma Y, Luo L and Wang H. Harmonizing economies and ecologies: towards an equitable provincial carbon quota allocation for china’s peak emissions. *Humanities and Social Sciences Communications*. 2024; 11(1): 1–10.